

Nonlinear evolution of the plasma beatwave: Compressing the laser beatnotes via electromagnetic cascading

Serguei Kalmykov* and Gennady Shvets

*Department of Physics and Institute for Fusion Studies,
The University of Texas at Austin, One University Station C1500, Austin, Texas 78712*

(Dated: August 14, 2018)

The near-resonant beatwave excitation of an electron plasma wave (EPW) can be employed for generating the trains of few-femtosecond electromagnetic (EM) pulses in rarefied plasmas. The EPW produces a co-moving index grating that induces a laser phase modulation at the difference frequency. The bandwidth of the phase-modulated laser is proportional to the product of the plasma length, laser wavelength, and amplitude of the electron density perturbation. The laser spectrum is composed of a cascade of red and blue sidebands shifted by integer multiples of the beat frequency. When the beat frequency is lower than the electron plasma frequency, the red-shifted spectral components are advanced in time with respect to the blue-shifted ones near the center of each laser beatnote. The group velocity dispersion of plasma compresses so chirped beatnotes to a few-laser-cycle duration thus creating a train of sharp EM spikes with the beat periodicity. Depending on the plasma and laser parameters, chirping and compression can be implemented either concurrently in the same, or sequentially in different plasmas. Evolution of the laser beatwave end electron density perturbations is described in time and one spatial dimension in a weakly relativistic approximation. Using the compression effect, we demonstrate that the relativistic bi-stability regime of the EPW excitation [G. Shvets, Phys. Rev. Lett. **93**, 195004 (2004)] can be achieved with the initially sub-threshold beatwave pulse.

PACS numbers: 52.35 Mw, 52.38 Kd, 52.38 Bv

I. INTRODUCTION

An electron plasma wave (EPW) is a natural tool for manipulating the properties of intense radiation beams. It can be used for up-shifting the laser frequency [1], for enhancing the self-focusing of co-propagating [2, 3] and counter-propagating [4] radiation beams, for the resonant self-modulation of the laser amplitude [5], and for coupling the signal and pump lasers in the parametric amplifier [6]. Also, the high-amplitude EPW driven by a short laser pulse can induce the pulse shrinkage with time [7].

Excitation of the EPW by the ponderomotive force (beatwave) of the two-color laser with the difference frequency Ω close to the electron Langmuir frequency $\omega_p = \sqrt{4\pi e^2 n_0 / m_e}$ (n_0 is an electron plasma density, m_e and $-|e|$ are the electron rest mass and charge) has attracted attention for a long time [8, 9, 10, 11]. The nonlinear plasma wave is highly sensitive to the variations of frequency and amplitude of the ponderomotive force. For example, by chirping the beat frequency [12] the EPW excitation can be enhanced by the autoresonance effect. Downshifting the beat frequency from the plasma resonance ($\Omega < \omega_p$) can also result in the large-amplitude wake excitation due to the effect of relativistic bi-stability [13, 14]. Conversely, the driven electron density perturbations can cause the laser amplitude modulation, either transverse [2, 3] or longitudinal [15]. Therefore, the performance of the beatwave scheme critically

depends on the self-consistent evolution of the light and plasma waves that includes effects of numerous plasma nonlinearities [16]. The relativistic self-phase modulation [17], stimulated forward Raman scattering [18, 19] (SFRS), and electromagnetic cascading [2, 3, 15, 20, 21] (EMC) broaden the laser frequency bandwidth, while the group velocity dispersion (GVD) of radiation distorts the laser amplitude. In certain regimes this scenario results in a strong local enhancement of the laser field. Specifically, the frequency downshifted ($\Omega < \omega_p$) beatwave pulse of initially low amplitude can be transformed into a train of sharp electromagnetic (EM) spikes of relativistic intensity and few-laser-cycles duration [15]. The spikes are separated in time by the beat period $\tau_b = 2\pi/\Omega$.

In the present paper a theoretical model is formulated which, in a weakly relativistic approximation, accurately describes the nonlinear excitation and relativistic bi-stability of the EPW, and frequency and amplitude modulation of the laser pulse in one spatial dimension (1D) and in time. We select specific regimes in which the EMC induced by near-resonantly driven EPW causes laser spectral broadening. At every point of the perturbed plasma, the EPW creates an index grating co-moving with the laser beams. Hence, the periodic frequency modulation (FM) of the laser develops at a difference frequency Ω . In spectral terms, the FM is manifested as a cascade of Stokes and anti-Stokes sidebands shifted by integer multiples of Ω from the laser fundamental ω_0 .

The effect of EMC has been known in physics of laser-plasma interactions since early 70s when Cohen *et al.* [20] suggested to enhance plasma heating by the decay of the cascade-driven EPW. Later on, the EMC was considered

*Electronic address: kalmykov@physics.utexas.edu

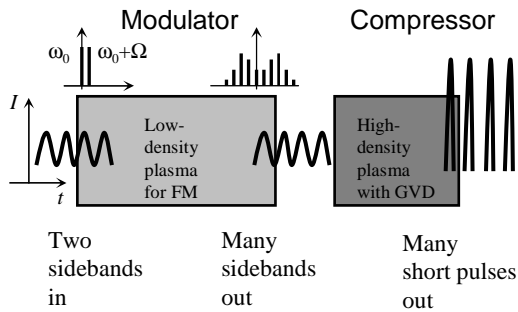


FIG. 1: Schematic of the two-stage cascade compressor. The frequency modulation (FM) occurs in a rarefied plasma. Denser plasma is used for the compression of beatnotes.

as an EPW diagnostic in the plasma beatwave accelerator [21]. Systematic study [2, 3] of plasma waveguiding options provided by the nonlinear interaction of laser beams with the cascade-driven EPW revealed an enhanced self-focusing of the co-propagating beams detuned in frequency below plasma resonance ($\Omega < \omega_p$). Calculations of Refs. [2, 3] describe the non-stationary cascade evolution in two dimensions (2D) in the planar and three dimensions (3D) in cylindrical geometry, take a full account of the relativistic nonlinearities of both cascade components and the EPW, but neglect the GVD of radiation and, hence, the longitudinal (temporal) distortion of the laser amplitude caused by the longitudinal transport of the cascade energy. Our work fills this gap by concentrating on the 1D compression of laser beatnotes due to the EMC and GVD.

We prove that the GVD completely dominates the evolution of weakly-relativistic beatwave (with intensity of initial beams over 10^{16} W/cm²) in either centimeter-scale rarefied ($n_0 \sim 10^{18}$ cm⁻³) or millimeter-scale dense plasmas ($n_0 \gtrsim 10^{19}$ cm⁻³). We show that the plasma wave driven *below* the plasma resonance, $\Omega < \omega_p$, chirps the laser frequency in a very special way: near the center of each laser beatnote the red-shifted sidebands are advanced in time with respect to the blue-shifted ones. The GVD can compress thus chirped beatnotes to a few-laser-cycle duration provided the laser bandwidth tends to ω_0 . The effect of GVD is controllable: proper adjustment of the plasma and laser parameters can reduce it while preserving the desirable bandwidth. In this case, the cascade compression can be made in two stages [15] (see Fig. 1): (i) a low-density plasma (the Modulator) with $\Omega < \omega_{p(M)}$ is used for the FM of initially two-frequency laser, and (ii) a higher-density plasma (the Compressor) with $\omega_{p(C)} \gg \Omega$ serves for the beatnote compression. Therefore, a train of sharp electromagnetic spikes of intensity by several orders of magnitude higher than ionization threshold for any medium can be generated. Similar concept of using Raman cascades for radiation beams compression in molecular gases has been successfully tested in experiments [22] at low laser intensities ($\ll 10^{14}$ W/cm²). The technique of the EMC compres-

sion in gases is not appropriate for applications requiring high laser intensity. One such application is using multiple short laser pulses with a tunable time delay for the coherent generation of plasma waves [23, 24, 25]. Making a sequence of several *independent* ultrashort high-intensity laser pulses with the periodicity of less than one picosecond could be a major experimental challenge [23]. The approach discussed in our paper suggests a viable path to creating such pulse trains at weakly relativistic intensity.

The outline of the paper is as follows. In Section II we derive the basic theoretical model (subsection II A) and analyze the basic scalings for the EMC and the cascade compression (subsection II B). In a realistic plasma, the EMC is a complicated interplay between the sideband coupling through the driven electron density perturbations, GVD of radiation, nonlinearities due to the relativistic increase of an electron mass, and SFRS. Fully nonlinear simulations presented in Sec. III account for all these effects and describe the cascade development in either two-stage (subsection III A) or single-stage (subsection III B) compressor. Because the longest time scale of the problem is only a few ion plasma periods, parametric decay of the EPW [26] and consequent plasma heating [20] are insignificant and thus ignored. The simulation parameters of subsections III A and III B are optimized so as to make the relativistic nonlinearities and SFRS almost negligible. When the parameters of the setup are not optimized, the SFRS can be seeded by the plasma wake driven by the beatwave pulse of finite duration. Contribution from the SFRS into the cascading process is discussed in the subsection III C. In the subsection III D we show how the beatnote compression helps in the EPW excitation via relativistic bi-stability [13] with the initially sub-threshold laser intensity. Conclusion gives the summary of the results. In Appendix A the amplitude of the plasma wake excited by a given detuned beatwave pulse is evaluated.

II. ONE-DIMENSIONAL THEORY OF EMC

A. Basic equations

We assume that the laser duration does not exceed a few ion plasma periods, so the ions are immobile and form a positive neutralizing background. In one spatial dimension and in the limit of weakly relativistic electron motion, Maxwell's equations and hydrodynamic equations of electron fluid give the coupled equations for the longi-

tudinal and transverse momentum of electrons [27]:

$$\left(\frac{\partial^2}{\partial t^2} + \omega_p^2\right) q_z = \frac{\omega_p^2}{2} q_z q^2 - \frac{c}{2} \frac{\partial^2 q^2}{\partial z \partial t} - c q_z \left(1 - \frac{q^2}{2}\right) \frac{\partial}{\partial z} \left(\frac{\partial q_z}{\partial t} + \frac{c}{2} \frac{\partial q^2}{\partial z}\right), \quad (1a)$$

$$\left(\frac{\partial^2}{\partial t^2} - c^2 \frac{\partial^2}{\partial z^2} + \omega_p^2\right) \mathbf{a} = \frac{\omega_p^2}{2} q^2 \mathbf{a} - c \mathbf{a} \left(1 - \frac{q^2}{2}\right) \frac{\partial}{\partial z} \left(\frac{\partial q_z}{\partial t} + \frac{c}{2} \frac{\partial q^2}{\partial z}\right). \quad (1b)$$

Here, $\mathbf{a} \equiv \mathbf{p}_{e\perp}/(m_e c)$ and $q_z \equiv p_{e_z}/(m_e c)$ are the normalized transverse and longitudinal components of the electron momentum, and $q^2 \equiv q_z^2 + \mathbf{a}_\perp^2 < 1$. We take $\mathbf{a} \equiv \text{Re}(\mathbf{e}_0 a)$, where $\mathbf{e}_0 = (\mathbf{e}_x + i\mathbf{e}_y)/\sqrt{2}$ is a unit vector of circular polarization; hence, $q^2 = q_z^2 + |a|^2/2$. In the 1D approximation, conservation of the transverse canonical momentum expresses the normalized momentum through the laser vector potential, $\mathbf{A}_\perp = (m_e c^2/e)\mathbf{a}$. The normalized electron density perturbation,

$$\frac{n_e - n_0}{n_0} \equiv \frac{\delta n}{n_0} \approx \frac{c}{\omega_p^2} \frac{\partial}{\partial z} \left[\frac{\partial q_z}{\partial t} + \frac{c}{2} \frac{\partial q^2}{\partial z}\right], \quad (2)$$

obeys the equation

$$\left(\frac{\partial^2}{\partial t^2} + \omega_p^2\right) \frac{\delta n}{n_0} - \frac{c}{2} \frac{\partial^2 q_z q^2}{\partial z \partial t} - \frac{c^2}{2} \frac{\partial^2 q_z^2}{\partial z^2} + c \frac{\partial^2}{\partial z \partial t} q_z \left(1 - \frac{q^2}{2}\right) \frac{\delta n}{n_0} = \frac{c^2}{4} \frac{\partial^2 |a|^2}{\partial z^2} \quad (3)$$

obtained through differentiating Eq. (1a) with respect to z and t . At the plasma entrance $z = 0$, the amplitude of a planar two-frequency laser beam is given by

$$a(0, t) = e^{-i\omega_0 t} [a_0(0, t) + a_1(0, t)e^{-i\Omega t}], \quad (4)$$

where $\Omega \approx \omega_p \ll \omega_0$. The ponderomotive beatwave [the right-hand side (RHS) of Eq. (3)] produces an electron density grating co-moving with the laser beams. The moving index grating produces the cascade of laser sidebands,

$$a(z, t) = e^{-i\omega_0 t + ik_0 z} \sum_{n=-\infty}^{+\infty} a_n(z, t) e^{-in\Omega t + ink_\Omega z}, \quad (5)$$

where $k_\Omega = \Omega/v_g$, and $v_g = k_0 c^2/\omega_0$ is the group velocity associated with the laser fundamental frequency. v_g is found from $d \equiv n_0/n_c = 1 - (v_g/c)^2$, where $n_c = m_e \omega_0^2/(4\pi e^2)$ is a critical plasma density. The amplitudes a_n vary slowly in time and space on scales Ω^{-1} and k_Ω^{-1} .

To describe the nonlinear evolution of the cascade (5), we take into account Eq. (2) and rewrite Eq. (1b) as

$$\left(\frac{\partial^2}{\partial t^2} - c^2 \frac{\partial^2}{\partial z^2}\right) a + \omega_p^2 a \left(1 - \frac{q^2}{2}\right) \left(1 + \frac{\delta n}{n_0}\right) = 0. \quad (6)$$

We retain in Eq. (6) the terms of order not higher than a^3 . Having in mind that $q_z \approx \delta n/n_0$, and that the relativistic saturation of the beatwave-driven EPW [8] occurs at $q_z \sim a^{2/3}$, we keep in Eq. (6) the nonlinear terms of order a^3 , $a q_z$, $a q_z^2$, $a q_z^3$ and finally arrive at

$$\left(\frac{\partial^2}{\partial t^2} - c^2 \frac{\partial^2}{\partial z^2} + \omega_p^2\right) a \approx \omega_p^2 (R^a + R^q - C). \quad (7)$$

The terms

$$R^a = a|a/2|^2, \quad (8a)$$

$$R^q \approx (a/2)(\delta n/n_0)^2(1 + \delta n/n_0) \quad (8b)$$

originating from the relativistic mass correction of an electron oscillating in the transverse (R^a) and longitudinal (R^q) fields describe the relativistic self-phase-modulation of laser. The leading nonlinear current term

$$C = a(\delta n/n_0) \quad (9)$$

is responsible for the EMC and stimulated forward Raman cascade [28]. Our earlier work [15] assumed the non-resonant EPW excitation ($\delta n/n_0 \sim a^2$), so the term (8b) was neglected. By including this term we include the regime with relativistic saturation of the resonantly driven EPW ($\delta n/n_0 \sim a^{2/3} \gg a^2$).

We substitute the expansion (5) into Eq. (7), replace the variables (z, t) by (z, ξ) (where $\xi/v_g = t - z/v_g$ is a retarded time, and z is the propagation distance through plasma), and collect the equal frequency terms. The resulting set of coupled envelope equations

$$\left[2i \frac{\omega_n}{v_g} \frac{\partial}{\partial z} - \frac{d}{v_g^2} (\omega_n - \omega_0)^2\right] a_n \approx k_p^2 (C_n - R_n^a - R_n^q), \quad (10)$$

where $k_p = \omega_p/c$, accounts for the propagation of sidebands through plasma [the first term in the left-hand side (LHS)], the GVD of the sidebands (the second term in the LHS), and the sideband coupling through the nonlinearities (the RHS). To evaluate the RHS of Eq. (10) we have to specify the nonlinear plasma response. The nonlinear electron density perturbation is driven by the ponderomotive force [the RHS of Eq. (3)] approximated as $-(c/2)^2 \sum_l (lk_\Omega)^2 \rho_l(z, \xi) e^{ilk_\Omega \xi}$. Here,

$$\rho_l = \sum_m a_m a_{m+l}^*, \quad (11)$$

and $|\partial \rho_l / \partial z| \ll k_\Omega |\rho_l|$. We expand the density perturbation in the ponderomotive force harmonics,

$$\delta n(z, \xi) = \frac{1}{2} \sum_l \delta n_l(z, \xi) e^{ilk_\Omega \xi}, \quad (12)$$

where $\delta n_{-l} = \delta n_l^*$, $|\delta n_l| \ll n_0$, and $|\partial \delta n_l / \partial \xi| \ll k_\Omega |\delta n_l|$, and assume that each density harmonic is driven by the corresponding harmonic of the ponderomotive force. In the expansion (12), the terms with $l = \pm 1$ are the closest

in frequency to the natural modes of plasma oscillations. They produce the dominant contribution to the cascade dynamics. Keeping in Eq. (3) the terms of order not higher than a^4 , and having in mind the scaling $|\delta n/n_0| \sim a^{2/3}$ that holds in the case of relativistic saturation of the resonantly driven EPW [8], we find that the amplitude $N_e \equiv \delta n_{-1}(z, \xi)/n_c$ obeys the nonlinear equation

$$\left(\frac{i}{k_\Omega} \frac{\partial}{\partial \xi} + \frac{\delta\omega}{\Omega} \right) N_e + R = \frac{d}{4} \rho_{-1}. \quad (13)$$

Here, $\delta\omega = (\Omega^2 - \omega_p^2)/(2\Omega)$ is the beatwave detuning from the plasma resonance, and R is proportional to the nonlinear frequency shift due to the relativistic mass increase of an electron oscillating in the longitudinal and transverse electric fields,

$$R = \frac{3}{16} N_e \left| \frac{N_e}{d} \right|^2 + \frac{1}{8} (\rho_0 N_e + \rho_{-2} N_e^*). \quad (14)$$

The initial condition for Eq. (13) is $N_e(z, -\infty) \equiv 0$ (unperturbed plasma ahead of the pulse). Amplitudes of the non-resonantly driven density harmonics ($l \neq \pm 1$) are found from the linearized Eq. (3):

$$\frac{\delta n_l(z, \xi)}{n_0} \approx \frac{1}{2} \frac{(\omega_l - \omega_0)^2}{(\omega_l - \omega_0)^2 - \omega_p^2} \rho_l(\xi, z). \quad (15)$$

Using equations (15), we evaluate the nonlinear terms in the cascade equations (10). We extract from the terms C a contribution from the EPW harmonics of orders $l \neq \pm 1$ and include it into the terms R^a . Therefore, only the contribution from the near-resonant EPW harmonic N_e determines the form of the ‘‘cascade’’ nonlinearity C_n . And, only near-resonant EPW harmonic is taken into account for evaluating the terms R_n^q . The result is

$$C_n = \frac{N_e a_{n-1} + N_e^* a_{n+1}}{2d}, \quad (16a)$$

$$R_n^a \approx \frac{1}{4} \sum_l a_{l+n} \rho_l - \frac{1}{4} \sum_l' a_{l+n} \rho_l \frac{(\omega_l - \omega_0)^2}{(\omega_l - \omega_0)^2 - \omega_p^2}, \quad (16b)$$

$$R_n^q \approx \frac{1}{4} \left[\left| \frac{N_e}{d} \right|^2 \left(a_n + \frac{3}{4} \frac{N_e}{d} a_{n-1} + \frac{3}{4} \frac{N_e^*}{d} a_{n+1} \right) + \frac{1}{2} \left(\frac{N_e}{d} \right)^2 \left(a_{n-2} + \frac{1}{2} \frac{N_e}{d} a_{n-3} \right) + \frac{1}{2} \left(\frac{N_e^*}{d} \right)^2 \left(a_{n+2} + \frac{1}{2} \frac{N_e^*}{d} a_{n+3} \right) \right]. \quad (16c)$$

The second term in the RHS of Eq. (16b) comes from the nonresonant EPW harmonics (15), prime means that the terms with $l = \pm 1$ are not included in the sum. The physical meaning of the nonlinearities (16) is as follows.

- The terms C_n couple the neighboring laser sidebands through the *near-resonantly-driven* harmonic of the EPW. These terms describe the electromagnetic cascading and the stimulated forward Raman cascade.
- The terms R_n^a describe the nonlinear frequency shifts produced by the relativistic mass increase of electron oscillating in the transverse fields and by the *nonresonantly-driven* harmonics of EPW.
- The terms R_n^q describe the nonlinear frequency shifts produced by the relativistic mass increase of electron oscillating in the longitudinal electric field of the *near-resonantly-driven* harmonic of the EPW. Only when the EPW is driven resonantly and reaches the relativistic saturation the term R_n^q can dominate R_n^a . In all the simulations that will follow in this paper R_n^q 's are negligibly small.

Assuming $v_g \approx c$, we rewrite the set (10) as

$$\left[\frac{2i}{k_0} \frac{\partial}{\partial z} - d \left(\frac{\omega_n - \omega_0}{\omega_0} \right)^2 \frac{\omega_0}{\omega_n} \right] a_n \approx d \frac{C_n - R_n^a - R_n^q}{\omega_n/\omega_0}. \quad (17)$$

The boundary condition for Eqs. (17) is given by Eq. (4). Equations (13) and (17) form the basis of 1D spatio-temporal weakly relativistic theory of the near-resonant plasma beatwave excitation. This theoretical model encompasses the phenomena of the nonlinear excitation and relativistic bi-stability of the EPW [13, 14], periodic FM of the laser [15, 22], GVD of the cascade components, and SFRS [18, 19, 28].

By the judicious choice of parameters the terms C_n can be made dominating in the RHS of Eq. (17), and laser spectral broadening will occur exclusively due to the EMC. Despite the large bandwidth of laser achieved in certain regimes of EMC, the effect of GVD can be negligible (see the discussion at the end of subsection IIB). The laser amplitude can be then modified in a separate, denser, plasma with the high GVD (the Compressor). In this two-stage scenario, nonlinearities of the Modulator affect primarily the laser phase, while in the Compressor the GVD modulates the amplitude. Compression of the laser beatnotes in plasma can result in the laser intensity so high as to give $|a|^2 \sim 1$.

The laser sidebands in Compressor remain coupled through the nonlinear frequency shifts, and the laser frequency bandwidth keeps growing. Thus, the relativistic nonlinearities of plasma can compete with the linear compression process. The Compressor density is chosen so as to entirely exclude the possibility of resonant plasma response: $\omega_{p(C)}$ is never close to an integer multiple of Ω . Provided $|n\rho_n| \ll 1$, the amplitude of density perturbation at the n^{th} beatwave harmonic is described by Eq. (15) with n_0 and ω_p replaced by $n_{0(C)}$ and $\omega_{p(C)}$. As the electron density perturbations in the Compressor are nonresonant and thus small, we neglect the terms R_n^q . Moreover, the terms C_n are absorbed by

R_n^a [that is, summation in the second term of Eq. (16b) is extended to $l = \pm 1$, and C_n 's do not show up in the Compressor equations]. We redefine the retarded time as $\zeta/v_{g(C)} = t - z/v_{g(C)}$ (where $v_{g(C)}$ is the group velocity of the laser fundamental component in the Compressor plasma of density $n_{0(C)} \gg n_0$) and find that the compression process can be described in terms of the coupled nonlinear equations similar to Eqs. (17):

$$\left[\frac{2i}{k_0} \frac{\partial}{\partial z} - d_C \left(\frac{\omega_n - \omega_0}{\omega_0} \right)^2 \frac{\omega_0}{\omega_n} \right] a_n \approx -d_C \frac{\omega_0}{\omega_n} R_n^{a(C)}. \quad (18)$$

Here, $d_C = n_{0(C)}/n_c \ll 1$ is the normalized Compressor density. The boundary conditions are given by the solution of Eqs. (17) at the Modulator exit, $a_n(z = z_{\mathcal{M}}, \xi)$.

B. Basic scalings for laser frequency modulation and compression

In the ideal two-stage compressor, the processes of EMC and compression are separated. The EMC develops in the Modulator plasma with zero GVD, while in the dense Compressor plasma with all the nonlinearities neglected the GVD compresses the radiation beatnotes. It is instructive to derive the basic scalings for each process because these approximate scalings will help to select the optimal parameters of fully nonlinear simulations.

When both R_n^a and R_n^q are taken to be zero, and the GVD is neglected ($d = 0$) in Eq. (17), scaling laws for the EMC are particularly simple. Assuming $\omega_n \approx \omega_0$, we derive from Eqs. (17) a set of conservation laws: $\partial \rho_l / \partial z = 0$. Hence, $\rho_l \equiv 0$ for $l \neq 0, -1$, $\rho_0(z, \xi) \equiv |a_0(0, \xi)|^2 + |a_1(0, \xi)|^2$, $\rho_{-1}(z, \xi) \equiv a_1(0, \xi) a_0^*(0, \xi)$, and, in the co-moving frame, N_e is independent of z despite the evolution of the laser phase. Thus simplified Eqs. (17) have the analytic solution [21]

$$a_n(z, \xi) = \sum_{\sigma=0,1} a_\sigma(0, \xi) e^{i(n-\sigma)(\psi+\pi)} J_{n-\sigma}(2W), \quad (19)$$

satisfying the initial condition (2) [here, $J_n(x)$ are the Bessel functions, and $\psi(z, \xi)$ and $W(z, \xi)$ are the phase and absolute value of the generating function $w(z, \xi) \equiv W e^{i\psi} = i(k_0 z/4) N_e(\xi)$]. Substituting Eq. (19) into Eq. (5) yields the expression for a train of phase-modulated beatnotes,

$$a(z, \xi) = \sum_{n=0,1} a_n(0, \xi) \cos[k_n \xi + \varphi(z, \xi)],$$

where $\varphi(z, \xi) = (k_0 z/2) |N_e(\xi)| \sin(\psi - k_\Omega \xi)$. The physical meaning of this result is that, without GVD, the laser undergoes frequency modulation only. The magnitude of the plasma wave depends only on the laser amplitude which remains unchanged. This is valid for any pair of $a_0(0, \xi)$, $a_1(0, \xi)$ and the corresponding $N_e(\xi)$.

The FM is periodic in time with the beat period τ_b when $N_e(\xi)$ is almost constant [this is the case for

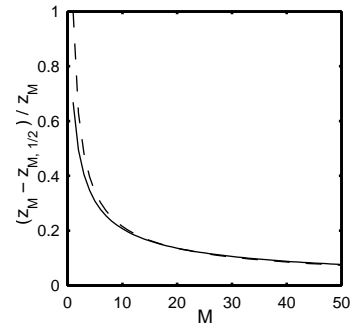


FIG. 2: Normalized distance between the points of the first maximum and half-maximum of $J_M(z)$ (solid line) and the scaling function $M^{-2/3}$ (dashed line).

$|\partial \rho_{-1} / \partial \xi| \ll |(\delta\omega/c) \rho_{-1}|$. To avoid the oscillations of N_e with time due to the relativistic dephasing [3, 8, 10], we take $|\delta\omega| \gtrsim 3(\omega_p/4) \sqrt[3]{3|\rho_{-1}|^2/2}$. Then, the term proportional to $\delta\omega$ dominates in the LHS of Eq. (13), which yields $N_e(\xi) \approx d|\rho_{-1}(\xi)/4|(\Omega/\delta\omega)$; then, for real $\rho_{-1}(\xi)$,

$$a = \sum_{n=0,1} a_n(0, \xi) \cos[k_n \xi + (k_0 z/2) N_e(\xi) \cos(k_\Omega \xi)]. \quad (20)$$

From equation (19), a Modulator plasma slab of thickness

$$z_{\mathcal{M}} \approx 2\mathcal{M}/(N_e k_0) \quad (21)$$

produces \mathcal{M} sidebands on either side of the fundamental, and a frequency bandwidth $\Delta\omega \sim 2\sqrt{d}\mathcal{M}\omega_0$. Conversely, $\mathcal{M} \sim r_e z_{\mathcal{M}} \lambda_0 |n_e - n_0|$, where $\lambda_0 = 2\pi c/\omega_0$ is the fundamental laser wavelength, and $r_e = e^2/(m_e c^2)$ is the classical electron radius.

As follows from Eq. (20), only for $\delta\omega < 0$ the laser wavelength decreases with time near the amplitude maximum of each beatnote (positive chirp). The GVD of plasma tends to compress thus chirped beatnotes: the shorter (blue-shifted) wavelengths catch up with the longer (red-shifted) wavelengths, eventually building up the field amplitude near the center of each beatnote. Thus, a sequence of sharp spikes is produced. If we consider an unperturbed Compressor plasma of given density, neglect the relativistic effects by setting $R_n^{a(C)} \approx 0$, and fix laser frequency and the number $2\mathcal{M}$ of satellites, we find that the peak compression occurs at a distance

$$z_C \approx \frac{\pi/3}{k_0 \mathcal{M}} \left(\frac{\omega_0}{\omega_{p(C)}} \right)^2 \left(\frac{\omega_0}{\Omega} \right)^2. \quad (22)$$

This estimate assumes that the outer sidebands were initially separated in time by roughly $\tau_b/2$ within one beatnote. To catch up with the red sidebands at the beatnote center, the blue sidebands need the propagation time $z_C/c \approx (c/\Delta v_g)(\tau_b/2)$, where the group velocity mismatch is $\Delta v_g \approx 2\mathcal{M}\Omega(\partial v_g/\partial\omega)_{\omega_0} \approx (3\mathcal{M}\Omega/k_0)(\omega_p/\omega_0)^2$.

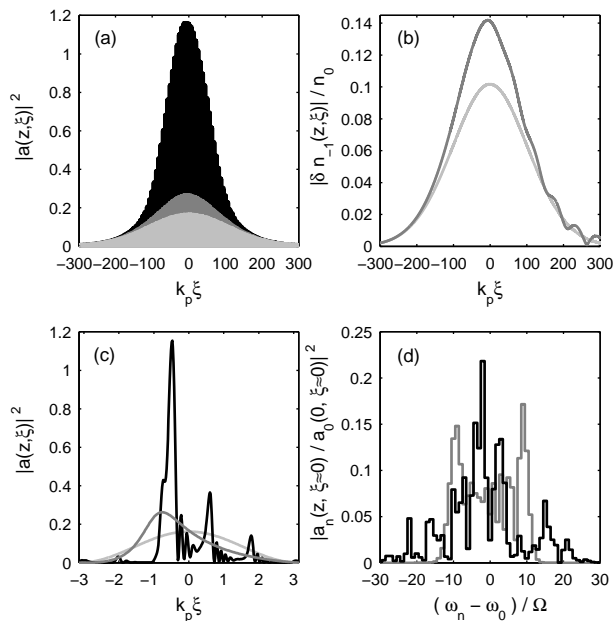


FIG. 3: The two-stage cascade compression. The physical quantities are shown at the entrance ($z = 0$, light gray) and exit of the Modulator ($z = z_8$, medium gray), and after the Compressor ($z = z_8 + z_C$, black). (a) The laser pulse intensity (the time window contains about 100 beatnotes). (b) The normalized amplitude of the near-resonant EPW, $\delta n_{-1}/n_0 = N_e/d$. (c) The beatnote intensity near the laser pulse center; one beat period near $\xi = 0$ is shown. (d) The laser spectra near $\xi = 0$. The nonlinearities and GVD in both plasmas are included.

The nonzero GVD of radiation in the Modulator plasma must be properly accounted for. The cascade components can be redistributed in time and space thus reducing coherence of the EPW excitation and affecting the frequency chirp. Naively, the GVD can become significant in the Modulator whose length z_M is close to the compression length estimated from Eq. (22) with $\omega_{p(C)} \equiv \omega_p$. However, the higher-order Stokes-anti-Stokes sidebands are generated later in plasma and have less time to catch up with the fundamental. Recalling that $|a_M| \propto |J_M(z)|$ in the Modulator, we define the half-growth length $z_{M,1/2}$ at which $|a_M|$ reaches a half of its maximum value, $|J_M(z_{M,1/2})| = |J_M(z_M)|/2$. Thereby, compression effectively takes place over the shorter distance $\Delta z \approx z_M - z_{M,1/2} < z_M$. The analytic formula $\Delta z \approx \mathcal{M}^{-2/3} z_M$ accurately fits Δz for $\mathcal{M} \gtrsim 5$ (see Fig. 2). Therefore, $\Delta z \ll z_M$ for $\mathcal{M} \gg 1$. Hence, for

$$z_M \ll \mathcal{M}^{2/3} z_C \approx (\lambda_0/6) \mathcal{M}^{-1/3} d^{-2}, \quad (23)$$

the effect of the GVD is negligible in the Modulator because the distance Δz actually available for the compression is less than z_C . Otherwise, if $z_M \gtrsim \mathcal{M}^{2/3} z_C$, the GVD in the Modulator becomes important.

Another manifestation of the GVD in the Modulator is the SFRS seeded due to finite duration of the beatwave

pulse. The stimulated forward Raman cascading [28] can interfere with the process of phase modulation and contaminate the laser frequency chirp. Reduction in the compression efficiency can follow. The effect of SFRS is examined in subsection III C.

III. NONLINEAR SIMULATIONS OF THE EMC

A. The two-stage cascade compressor

We model the EMC by numerically solving the set of coupled nonlinear equations (13) and (17) with the boundary condition

$$a_0(0, \xi) = a_1(0, \xi) = A e^{-\xi^2/(c\tau_L)^2} \quad (24)$$

for the laser sidebands, and $N_e(z, \xi = -\infty) \equiv 0$ for the EPW. The beatnote compression in the second stage is modeled by numerically solving the Compressor equations (18). All the nonlinearities associated with the effects of relativistic mass correction and non-resonant electron density perturbations are retained in the modeling of both stages. In all the simulations below, the fundamental laser wavelength is fixed at $\lambda_0 = 0.8 \mu\text{m}$.

The two-stage compression starts with the initial laser amplitude $A = 0.2$, the Modulator density $n_0 = 8.75 \times 10^{17} \text{ cm}^{-3}$ (hence, $d = 5 \times 10^{-4}$), and $\delta\omega = -0.1\omega_p$. The laser pulse duration is $\tau_L = 4.5 \text{ ps}$ (about half the ion plasma period for a fully ionized Helium). Having chosen the maximum density perturbation $|N_e(z = 0)|_{\text{max}} \approx 0.5 \times 10^{-4}$ and resulting spectral width of the laser ($\mathcal{M} \approx 8$ sidebands on each side), we find the Modulator length $z_8 \approx 4.1 \text{ cm}$ (such interaction length could be implemented in a plasma channel [29]).

The simulation results are shown in Fig. 3. From the plot (a) it is seen that the peak laser intensity at the Compressor exit ($z = z_8 + z_C$) is by a factor of 7.2 larger than at the Modulator entrance ($z = 0$). The increase in intensity results from the shown in plot (c) beatnote compression from the initial duration of $\tau_{b(in)} \approx 120 \text{ fs}$ to $\tau_{b(out)} \approx 13 \text{ fs}$ (roughly 5 laser cycles). Compressor plasma has the density $n_{0(C)} = 25n_0$ and length $\approx 0.0275z_8 \approx 1.1 \text{ mm}$ (such a short dense plasma can be created by ablation of a microcapillary [30]).

The inequality (23) is very well satisfied for the Modulator parameters. Consequently, the beatnote pre-compression seen in the plot (c) is quite insignificant. Plot (b) shows that $N_e(z, \xi)$ also reveals almost negligible variation with z in the Modulator. Thereby, according to the plots (b) and (c), the EMC develops in accordance with the scenario outlined in subsection II B.

Compression in the second stage clearly proceeds in the nonlinear regime. The laser amplitude becomes relativistic ($|a| \rightarrow 1$), and the nonlinear frequency shifts in Eqs. (18) couple the laser sidebands and further increase the laser bandwidth. Figure 3(d) shows that the resulting frequency spectrum is at least twice as broad if compared with that at the Modulator exit. As a consequence,

the linear formula (22) overestimates z_C by a factor of three since it ignores both pre-compression of the pulse in the Modulator and additional bandwidth increase in the Compressor. Also, quality of the compressed beatnotes is not perfect: instead of a single sharp spike, one can observe a multi-spike structure in Fig. 3(c), the distance between the spikes being roughly $\tau_b/5$. One can relate this structure to the phase modulation occurring due to the electron density perturbation at fifth harmonic of the beatwave frequency, which is the closest to the natural mode of the Compressor plasma oscillations. Due to this effect, one beatnote is not gradually compressed into one spike but rather splits into five spikes, of which the one located near the original beatnote maximum has the largest amplitude.

A number of issues are yet to be addressed before the theory of the cascade compression is complete. The neglected effects of transverse evolution of the laser, such as relativistic self-focusing and cascade focusing [3], are dominant at high plasma density in the Compressor and are potentially adverse. But, we find the 1D scenario of the two-stage compression conceptually simple and useful for understanding the underlying phenomena. In the next subsection we consider the single-stage approach which assumes concurrent cascading and compression in the same low-density plasma.

B. The single-stage cascade compressor

Increasing plasma density in the Modulator increases the GVD. Therefore, we can explore the idea of compressing the beatnotes concurrently with generating the sidebands. In the following set of simulations the electron density is doubled, $n_0 = 1.75 \times 10^{18} \text{ cm}^{-3}$. Cascade compression is simulated in plasma of the same length, $z_8 = 4.1 \text{ cm}$, and with the same initial density perturbation $|N_e(z=0)|_{\text{max}} \approx 0.5 \times 10^{-4}$ as in the previous subsection. The laser amplitude is $A \approx 0.071$, and the beatwave detuning is $\delta\omega = -0.025\omega_p$. As we shall see in subsection III C, the SFRS manifestation can be large in this regime. Appropriately low seed level can be achieved with the beatwave pulse envelope varying slowly on the time scale $\delta\omega^{-1}$. We choose the beatwave pulse $\tau_L = 14.25 \text{ ps}$ long (which is about three ion plasma periods for a fully ionized Helium), which corresponds to $|\delta\omega\tau_L| \approx 27$. The given initial intensity on axis and laser duration require the pulse energy of about 5 J in the focal spot of 30 μm radius.

The linear estimate of the effective compression length (22) shows that the inequality (23) almost breaks under the simulation parameters. Hence, a beatnote compression is large at the plasma exit. Figure 4(a) shows that the resulting peak intensity is by an order of magnitude larger than at the plasma entrance. Initial duration of the laser beatnote, as shown in Fig. 4(c), is reduced from $\tau_{b(in)} \approx 85 \text{ fs}$ by roughly a factor of 10 (to roughly 3 laser cycles). The spectral features of the

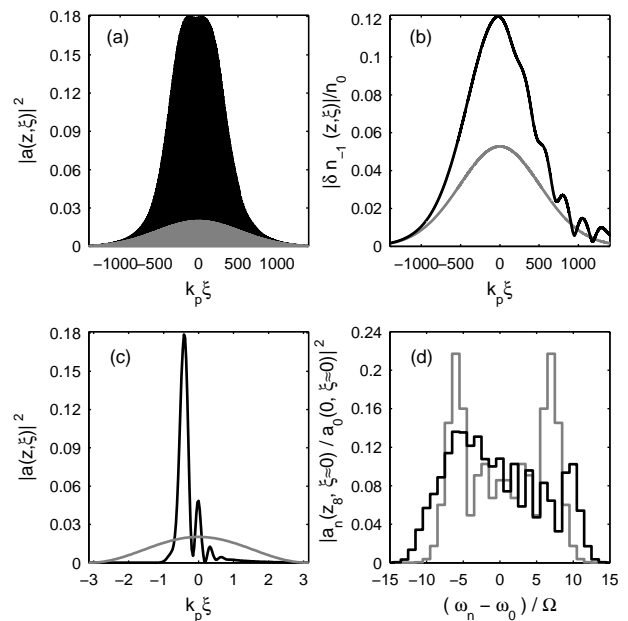


FIG. 4: The single-stage compressor with concurrent EMC and compression. In plots (a) - (c), the physical quantities are shown at the entrance ($z = 0$, gray) and exit of the plasma ($z = z_8$, black). (a) The laser pulse intensity (the time window contains about 500 beatnotes). (b) The normalized amplitude of the near-resonant EPW, $\delta n_{-1}/n_0 = N_e/d$. (c) The beatnote intensity near the laser pulse center, $\xi = 0$. (d) The laser spectra near $\xi = 0$ with (black) and without (gray) GVD and all nonlinear frequency shifts.

EMC are different from those obtained with the nonlinear frequency shifts and the GVD neglected [i.e., with $d = 0$ in Eqs. (17)]. A red asymmetry of the cascade spectrum is seen in Fig. 4(d). Some spectral broadening versus the case of $d = 0$ can be attributed to the self-phase-modulation produced by the nonlinear frequency shifts. Figure 4(b) shows that the electron density perturbation is not an integral of motion. Its final amplitude is roughly twice the initial, and a small-amplitude wake is left behind the train of compressed spikes which can be recognized as a signature of SFRS. Despite of this, neither the self-phase-modulation nor the SFRS are adverse for the cascade compression.

The transverse evolution of the cascade is a matter of high importance for the experimental verification of this compression scheme. For instance, electron density perturbations can significantly lower the nonlinear focusing threshold of counter-propagating laser beams [4]. The co-propagating cascade of electromagnetic beams also experiences enhanced focusing in both 2D (planar) and 3D (cylindrical) geometry if $\Omega < \omega_p$ (Refs. 2, 3). We shall give here a few necessary estimates (effects of transverse evolution will be given a detailed consideration in the upcoming publications). When the beatwave is downshifted by $\delta\omega = -3(\omega_p/4)\sqrt[3]{3|\rho_{-1}|^2/2}$, the self-focusing threshold in the planar 2D geometry [2, 3]

is $a_0(k_p x_0/10)^3 \geq 0.064$, where x_0 is a laser focal spot size ($a_0 = a_0 e^{-x^2/x_0^2}$). So, the sub-threshold regime under the parameters of Figs. 3 and 4 requires the spot size $x_0 < 40 \mu\text{m}$. If we loosely translate x_0 into the radius of the laser focal spot in the cylindrical geometry, we find that the refraction-limited interaction length $2z_R = (2\pi/\lambda_0)x_0^2$ is less than 1.2 cm. However, the required $z_8 \approx 4.1$ cm can be achieved by means of the plasma channel guiding [29].

In the regime of cascade compression considered above, eliminating potentially adverse effects of laser self-phase-modulation and SFRS required complying with some hard restrictions on the laser pulse amplitude, duration, and beatwave frequency detuning ($|a|^2 \ll 1$, and $|\delta\omega\tau_L| \gg 1$). The next set of simulations shows that these conditions are desirable but not necessary for the manifestation of the effect. The cascade compression can be observed even for ultrashort (~ 100 fs) beatwave pulses propagating in a dense plasma ($n_0 \sim 10^{19} \text{ cm}^{-3}$) where neither GVD nor relativistic nonlinearities are small. We consider the evolution of a two-color ultrashort laser [31] whose energy is initially distributed between the fundamental (97%) and the Stokes (3%) components. The laser frequencies are $\omega_0 = 2.356 \times 10^{15} \text{ s}^{-1}$ ($\lambda_0 = 0.8 \mu\text{m}$) and $\omega_1 = 2.159 \times 10^{15} \text{ s}^{-1}$ ($\lambda_1 = 0.873 \mu\text{m}$). Assuming that $\omega_0 - \omega_1 = 0.95\omega_p$, we derive the plasma density $n_0 = 1.35 \times 10^{19} \text{ cm}^{-3}$; hence, $d = 7.725 \times 10^{-3}$. We choose $a_0 \approx 0.3$, and $a_1 \approx 0.048$. At $z = 0$, the laser pulse is Gaussian (24) with a duration $\tau_L \approx 90$ fs. In this case $|\delta\omega\tau_L| \approx 0.9$, and the beatwave pulse amplitude is not slowly varying. Nevertheless, under these seemingly unfavorable conditions, the EMC develops very effectively and the intensity contrast of the amplitude-modulated laser pulse grows rapidly. The plasma length is chosen so as to produce 5 sidebands on either side; the plasma length is bounded from above by $z_5 \approx 2.5$ mm, while the compression length evaluated from formula (22) for $\mathcal{M} = 5$ gives the lower bound, $z \approx 0.45$ mm. The most spectacular features of the EMC shown in Fig. 5 are observed at $z \approx 1.8$ mm. At the plasma border, $z = 0$, the intensity variation of the two-color laser is about 50%, while at $z \approx 1.8$ mm very deep amplitude modulation develops with the intensity contrast ratio reaching a factor of 25. The mostly affected are the beatnotes in the tail of the laser pulse; they are compressed to roughly a quarter of a plasma period. The laser nonlinear evolution boosts the amplitude of the plasma wake (which is increased by a factor of 3). The laser spectrum broadens and reveals a red shift by about $-\omega_0/2$. This is a clear indication of the forward stimulated Raman cascade [28] which, as appears in this simulation, does not prevent the beatnote compression. Moreover, the laser frequency red-shifts towards the pulse tail. The red-shifted field components that form the compressed beatnotes in the tail move slower than those in the pulse head. Thus, as seen in Fig. 5(a), the beatnotes in the tail accumulate a considerable time delay (about a quarter of the beat period) with respect to the initial positions of their max-

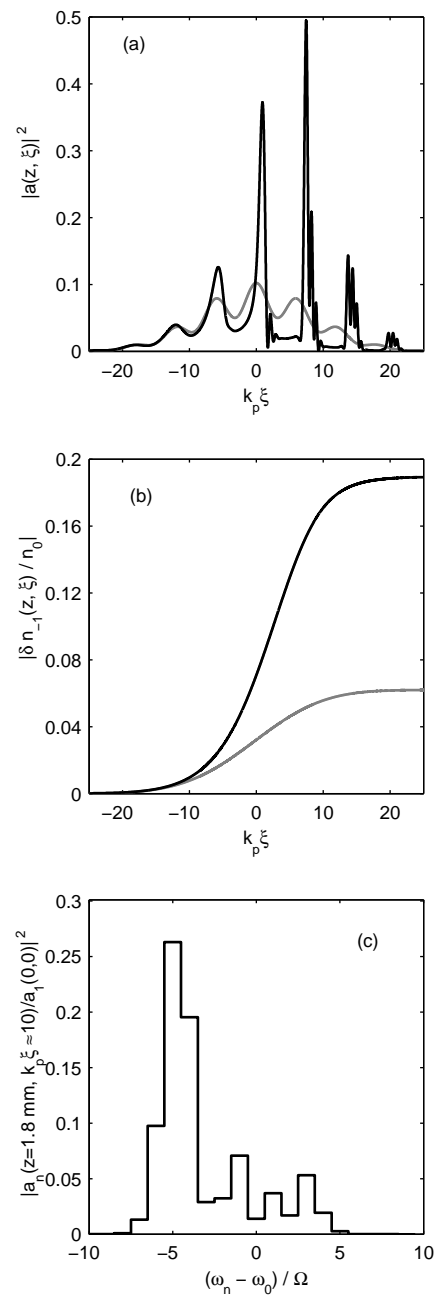


FIG. 5: The EMC of the two-color short-pulse (90 fs) laser [31] in a dense ($1.35 \times 10^{19} \text{ cm}^{-3}$) plasma. Physical quantities are shown at the plasma entrance ($z = 0$, gray lines) and exit ($z = 1.8$ mm, black lines).

ima. This time delay is in agreement with the frequency shift $-\omega_0/2$.

The simulations presented in this subsection demonstrate the robustness of the EMC in the conditions when the GVD is large, and the nonlinear processes of the relativistic self-phase modulation and the SFRS interfere the cascading process. Slow variation of the beatwave pulse envelope is therefore helpful but not necessary for the cascade compression.

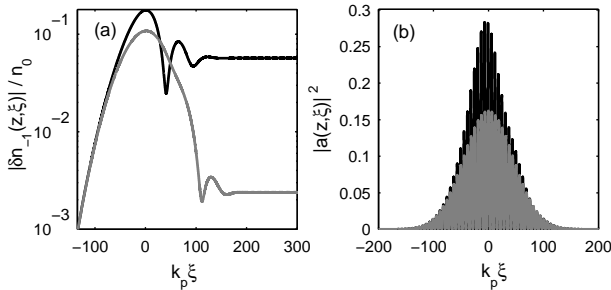


FIG. 6: Electron density perturbation (a) and the temporal profile of laser intensity (b) for the parameters the same as of Fig. 3 except the laser duration reduced by a factor of 2.5, $\omega_p \tau_L \approx 100$. Gray color — $z = 0$, black — $z = z_8$.

C. Manifestation of SFRS in cascade compressor

Equations (17) admit the longitudinal transfer of electromagnetic energy in the co-moving frame. Therefore, the laser amplitude modulation may result not only from the EMC with concurrent compression of beatnotes but also as a consequence of the SFRS instability [18, 19, 28] (also referred to as the 1D resonant modulational instability [5]). The SFRS is different from the EMC. The latter is merely a phase modulation which may proceed in the absence of GVD.

The SFRS is a resonant process seeded by the electron density perturbations oscillating at the plasma frequency ω_p . The instability bandwidth is much narrower than ω_p even in the case of relativistically strong pump, $a_0 \sim 1$ (Ref. [19]). And, in the examples of Figs. 3 and 4, the SFRS bandwidth is much lower than the absolute value of the beatwave frequency detuning $\delta\omega$. However, an electron plasma response to the laser beatwave *always* contains a component oscillating at ω_p . This component is due to the finite duration of the beatwave pulse, and its amplitude is governed by the product $|\delta\omega\tau_L|$. These resonant density perturbations can be enhanced by the SFRS to a level comparable to that of a non-resonant plasma response, and can interfere the phase modulation process. Hence, the effect of the SFRS is adverse and should be avoided by the judicious choice of laser and plasma parameters.

The seed level for the SFRS can be reduced by taking $|\delta\omega\tau_L| \gg 1$. For example, parameters used in Figs. 3 and 4 correspond to $|\delta\omega\tau_L| \sim 30$ and reveal no SFRS manifestation: no considerable plasma wake is left behind the laser at $z = z_8$. Hence, the plasma response is almost entirely non-resonant in these simulations.

Under parameters of Fig. 3, reduction in the beatwave pulse duration by a factor of 2.5 ($|\delta\omega\tau_L| = 10$) produces visible enhancement of the plasma wake that can be attributed to the SFRS manifestation (see Fig. 6). At the plasma border, the wake amplitude is $\delta n(z=0) \equiv \delta n_s \approx 2.4 \times 10^{-3} n_0$. Taking δn_s as the SFRS seed amplitude, we can theoretically evaluate the am-

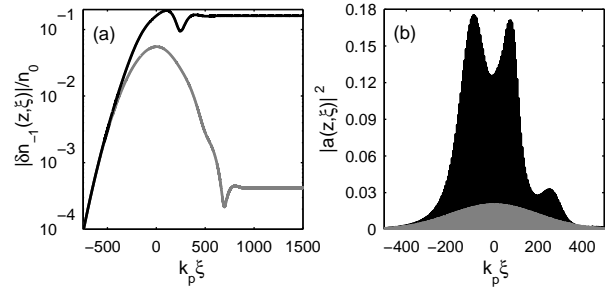


FIG. 7: Electron density perturbation (a) and the temporal profile of laser intensity (b) for the parameters the same as of Fig. 4 except the laser duration reduced to $\omega_p \tau_L \approx 440$, and $|\delta\omega\tau_L| = 10$. Gray color — $z = 0$, black — $z = z_8$.

plification factor by using the formula (4.12) of Ref. [19], $\ln |\delta n(z)/\delta n_s| \approx (2/c)(z \int_{-\infty}^{+\infty} \Gamma_0^2(\tau) d\tau)^{1/2}$. This expression takes into account the laser temporal profile and is valid for $z \gg \xi \gg c\tau_L$; $\Gamma_0^2(\tau) = (1/8)(\omega_p^4/\omega_0^2)a_0^2(\tau)$ stands for the instantaneous growth rate. The theoretical estimate of amplification factor is $\ln |\delta n(z_8)/\delta n_s| \approx 3.36$. On the other hand, comparing the wake amplitudes at the entrance ($z = 0$) and at the exit ($z = z_8$) of the plasma gives the amplification factor of $\ln |\delta n(z_8)/\delta n_s| \approx 3.2$, which is very close to the analytical estimate. We have found that the theory and simulation agree for $80 < \omega_p \tau_L < 300$. Therefore, throughout this range, plasma wakes are excited almost entirely by the SFRS. Remarkably, the maximum laser intensity, as well as the shape of individual beatnotes, is almost the same at $z = z_8$ for the parameters of Figs. 3 and 6. Hence, in the considered parameter range the effect of SFRS has a negligible effect on the laser evolution.

Oppositely to the just discussed case of rarefied plasma, reducing the laser duration by the same factor 2.5 under the parameters of Fig. 4 (i.e., plasma twice as dense versus that of Figs. 3 and 6) causes significant enhancement of SFRS. Figure 7(a) shows the plasma wake amplification by a factor of $\ln |\delta n(z_8)/\delta n_s| \approx 6.05$. Theoretical estimate of the SFRS gain gives 4.2; this discrepancy can be partially explained by the laser amplitude growth due to the beatnote compression. Figure 7(b) demonstrates the strong deformation of the beatwave intensity profile. The spectral content of the electromagnetic cascade varies considerably and can exhibit either overall red- or blue-shift at different ξ in the window $-100 < k_\Omega \xi < 100$.

In conclusion, to get rid of the SFRS, one should keep the SFRS seed low by keeping the product $|\delta\omega\tau_L|$ large. As the simulations show, it should be larger than 20; this may require the beatwave pulse duration of several picoseconds or larger.

D. Relativistic bi-stability of EPW

Cascade compression is a perfect tool for studying threshold phenomena. One of them, the relativistic bi-stability (RB) of the EPW driven by the long ($|\delta\omega\tau_L| \gg 1$) beatwave pulse with $\Omega < \omega_p$, is considered in this subsection. The RB results in the excitation of large-amplitude plasma wakes [13]. The intensity threshold should be met for the RB to occur. The threshold is multi-faceted: it is determined by the beatwave frequency detuning $\delta\omega$, the laser amplitude, shape, duration, contribution from the plasma wave harmonics *etc.* Various aspects of the RB in the approximation of the given driver $\rho_{-1}(\xi)$ are addressed in the forthcoming publication [14].

Evolution of the laser amplitude becomes important when a laser propagates over a considerable distance in the plasma. Strong distortion of the beatwave temporal profile within a finite distance (few millimeters) in a dense ($n_0 \sim 10^{19} \text{ cm}^{-3}$) plasma does have adverse consequences for the amplitude- and phase-sensitive process of RB. On the other hand, we demonstrate below that the beatnote compression helps to cross the RB threshold in the case of initially sub-threshold laser amplitude. We start the simulation with the parameters of the numerical example from Ref. [13]: simulation starts at $z = 0$ in a plasma with a density $n_0 = 10^{19} \text{ cm}^{-3}$, the beatwave pulse having a Gaussian temporal profile (24) with $\omega_p\tau_L \approx 212$ and $\delta\omega = -0.05\omega_p$, and the laser fundamental wavelength being $\lambda_0 = 0.8 \text{ } \mu\text{m}$ (then, $d \approx 0.0057$). Solution of Eq. (13) with a given driver (equivalent to the calculations of plasma response at the entrance point $z = 0$) show that the RB threshold is $A^2 \approx 0.03375$ (16% lower than in Ref. 13). This threshold corresponds to the normalized peak intensity $|a|_{\text{max}}^2 \approx 0.135$. To demonstrate how this threshold is crossed in the course of laser evolution in plasma, we start the simulation with a sub-threshold value of the laser intensity, $A^2 \approx 0.027$. The simulation results are shown in Fig. 8.

As the laser travels through plasma, the cascade compression of the beatnotes locally increases the intensity, and the RB threshold is crossed at a distance $z \approx 0.53 \text{ mm}$. At this point, the magnitude of the electron density perturbation jumps abruptly by a factor of 2.3 [$\delta n_{-1}/n_0$ immediately before and after crossing the RB threshold is shown in Fig. 8(a)]. After that point, the resonant density perturbation grows steadily to roughly 80% of background density. At $z \approx 1.2 \text{ mm}$ the beatwave amplitude distortion becomes so strong as to destroy the coherence of the plasma response, and δn_{-1} drops sharply. Importantly, at the point where the RB threshold is met, the beatnote amplitude is not very different from sinusoidal [see the inlay in Fig. 8(b)], and the shape of the beatwave pulse is not much different from the initial Gaussian. The normalized intensity at which the RB occurs in the simulation is $|a|_{\text{max}}^2 \approx 0.145$. The amplitude of the beatwave pulse immediately before ($z = 0.52 \text{ mm}$) and after ($z = 0.54 \text{ mm}$) crossing

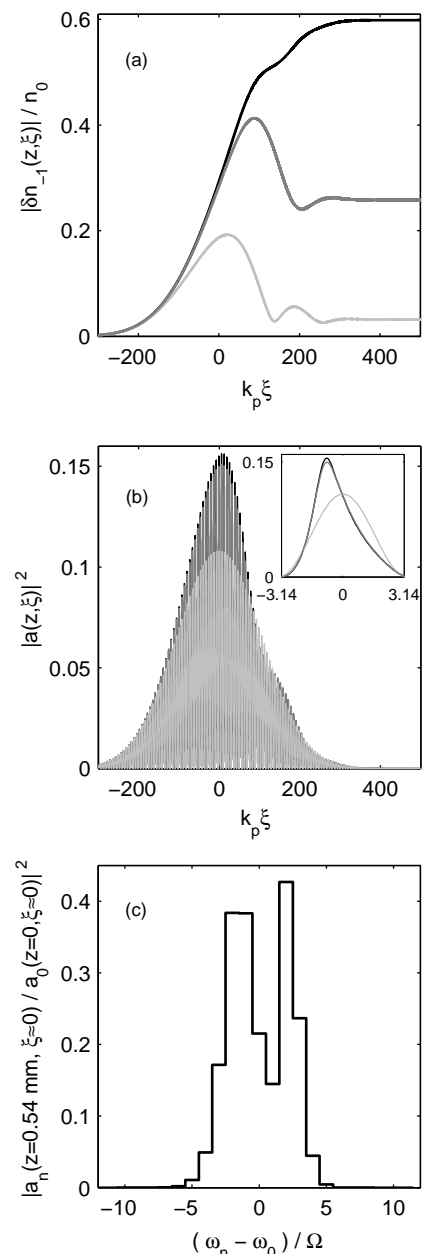


FIG. 8: Relativistic bi-stability of the EPW. Magnitude of the near-resonant electron density perturbation [plot (a)] and the laser intensity [plot (b)] are shown at $z = 0$ (light gray), $z = 0.52 \text{ mm}$ (medium gray), and $z = 0.54 \text{ mm}$ (black). Inset in plot (b): one beatnote selected near $\xi = 0$. Plot (c): the laser spectrum at $z = 0.54 \text{ mm}$. The RB threshold is crossed at $z \approx 0.53 \text{ mm}$. Crossing the threshold increases the EPW amplitude by a factor of 2.3.

the RB threshold is almost the same, as can be seen in the plot 8(b). As follows from Fig. 8(c), the beatnote compression necessary for reaching the RB threshold is achieved at the laser bandwidth roughly equal to $\omega_0/3$.

Therefore, the proposed model of EMC in plasmas with nonzero GVD is able to demonstrate the effect of rela-

tivistic bi-stability in the dynamic simulations with initially sub-threshold laser amplitude.

IV. CONCLUSION

In this paper, we have developed a nonlinear model that describes the evolution of laser beatwave and electron density perturbations in time and in 1D in space in the weakly relativistic regime. Electromagnetic spectrum evolution and the effects of finite group velocity dispersion are accurately modeled. The model includes the nonlinear frequency shifts related to the relativistic corrections of electron mass and the harmonics of the electron density perturbations. It also takes into account the spatio-temporal evolution of the near-resonantly driven electron density perturbation. The theoretical model also describes a number of nonlinear effects important for the implementation of plasma beatwave accelerator. It is found that, for the beatwave downshifted in frequency from the plasma resonance, the electromagnetic cascading produced by the near-resonant electron density perturbations leads to the compression of the laser beatnotes, which finally transforms the beatwave pulse into a train of sharp (few-laser-cycle) electromagnetic spikes separated by the beat period in time and space. A train of electromagnetic pulses useful for the particle acceleration applications [23, 24, 25] can be self-consistently created. We are also able to demonstrate how the electron plasma wave of large amplitude can be excited due to the effect of relativistic bi-stability even in the case of initially sub-threshold beatwave pulse. The work is supported by the U.S. Department of Energy under Contracts No. DE-FG02-04ER54763 and DE-FG02-04ER41321, by the National Science Foundation grant PHY-0114336 administered by the FOCUS Center at the University of Michigan, Ann Arbor.

APPENDIX A: ELECTRON DENSITY PERTURBATION DRIVEN BY A GIVEN BEATWAVE PULSE

In this Appendix we evaluate analytically and numerically the initial density perturbations in the ranges of laser parameters (amplitude, duration, and the beat frequency) relevant to the numerical examples of this paper. We consider the excitation of EPW at the plasma border $z = 0$ and take the Gaussian temporal profile of laser 24. Then, the normalized amplitude $\varepsilon(t) = \delta n(t)/n_0$ of near-resonantly driven electron density perturbation obeys the weakly nonlinear equation

$$[\Omega^{-1}\partial/\partial t - i\delta\omega(t)]\varepsilon = -i(A/2)^2 e^{-2t^2/\tau_L^2}, \quad (\text{A1})$$

where $\delta\omega(t) = \delta\tilde{\omega} + (3/16)|\varepsilon(t)|^2 + (A/2)^2 e^{-2t^2/\tau_L^2}$, $\delta\tilde{\omega} = \delta\omega/\Omega$, $|\delta\omega(t)| \ll 1$. We will solve this equation numerically with the initial condition $\varepsilon(-\infty) = 0$ (plasma is quiescent before the laser pulse arrival).

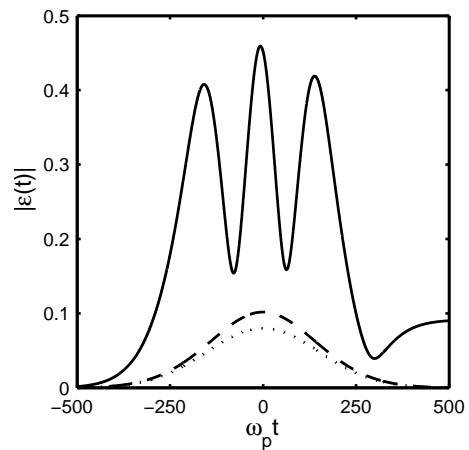


FIG. 9: Temporal evolution of the EPW driven by the two-frequency laser pulse of duration $\omega_p\tau_L = 300$. The laser intensity profile $|a_0(t)|^2 + |a_1(t)|^2$ is shown with a dotted line. Numerical solution to Eq. (A1) gives the EPW amplitude in the resonant ($\Omega = \omega_p$, solid line) and near-resonant ($\Omega = 0.9\omega_p$, dashed line) cases.

Note, that Eq. (A1) can be solved analytically by means of the perturbational approach when $|\delta\tilde{\omega}_l| > \Delta \equiv (1/2)\sqrt[3]{3(A/2)^4}$ (Ref. [10]), and $\delta\omega\tau_L \gg 1$. Then, $\varepsilon(t)$ adiabatically follows the temporal profile of ponderomotive force, and, in the zero-order approximation, the time derivative can be omitted in Eq. (A1). First-order approximation is obtained via linearization of Eq. (A1) with $|\varepsilon(t)|^2 \approx [(A/2)^4/\delta\tilde{\omega}^2]e^{-4t^2/\tau_L^2}$. The solution reads

$$\varepsilon(t) \approx -i(a/2)^2 e^{i\delta\omega t - i\Omega\tau_L\Phi(t)} \times \int_{-\infty}^t e^{-2\tau^2/\tau_L^2 - i\delta\omega\tau + i\Omega\tau_L\Phi(\tau)} d\tau, \quad (\text{A2})$$

where $\Phi(x) = \kappa_1 \text{erfc}(2x/\tau_L) + \kappa_2 \text{erfc}(\sqrt{2}x/\tau_L)$, $\text{erfc}(y) = (2/\sqrt{\pi}) \int_y^{+\infty} e^{-t^2} dt$, $\kappa_1 = (3\sqrt{\pi}/64)(A/2)^4/\delta\tilde{\omega}^2$, and $\kappa_2 = \sqrt{\pi/8}(A/2)^2$.

Figure 9 illustrates the evolution of the EPW amplitude for the resonant ($\Omega = \omega_p$) and near-resonant ($\Omega = 0.9\omega_p$) excitation. In the near-resonant case, the beatwave pulse amplitude varies slowly: $|\delta\omega\tau_L| \approx 30$. Resonant plasma beatwave [numerical solution of Eq. (A1)] exhibits oscillations due to the periodic dephasing produced by the relativistic frequency shift [8, 10]. This effect is eliminated by introducing the detuning $\delta\tilde{\omega} \approx -3\Delta = -0.1$ (compare dashed and solid curves in Fig. 9). Under parameters of Fig. 9, $\delta\tilde{\omega}$ dominates the relativistic frequency shifts $[(3/16)|\varepsilon(t)|^2 < 0.002$ and $|a_0(t)/2|^2 \leq 0.01]$, and the numerical solution of Eq. (A1) almost coincides with the analytic approximation (A2).

The amplitude of the seed plasma wave from which the SFRS can grow inside plasma can be estimated using the the amplitude of wake plasma wave left behind the laser, $|\varepsilon(t \rightarrow +\infty)|$. We evaluate it numerically from Eq. (A1) and plot as a function of τ_L for various negative detunings

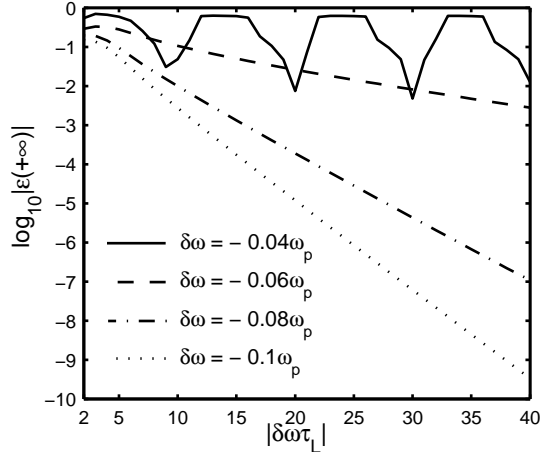


FIG. 10: Amplitude of the plasma wake excited by the detuned beatwave as a function of laser pulse duration; $a^2 = 0.04$.

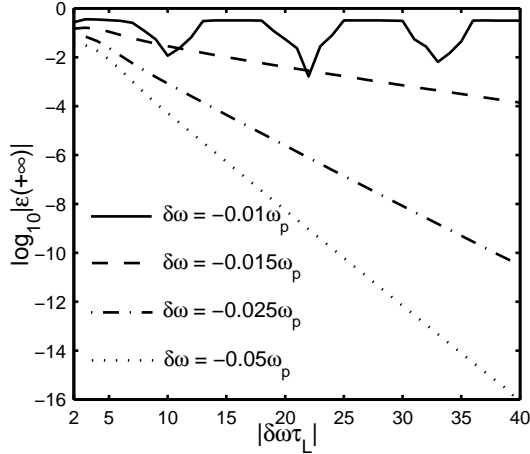


FIG. 11: Amplitude of the plasma wake excited by the detuned beatwave as a function of laser pulse duration; $a^2 = 0.005$.

$\delta\omega$ in Figs. 10 (with the maximal laser intensity as of Fig. 3) and Fig. 11 (with the maximal laser intensity as of Fig. 4). For the large negative detunings ($\delta\omega < -0.055\omega_p$ for Fig. 10, and $\delta\omega < -0.0125\omega_p$ for Fig. 11) the plasma wake amplitude drops with τ_L monotonously, while for smaller magnitudes of $|\delta\omega|$ (numerical examples are given for $\delta\omega = -0.04\omega_p$ in Fig. 10, and for $\delta\omega = -0.01\omega_p$ in Fig. 11) it exhibits an oscillatory behavior. As the pulse duration τ_L grows, the wake amplitude periodically reaches the value $|\varepsilon(t \rightarrow +\infty)| \approx 0.7$ (Fig. 10) and $|\varepsilon(t \rightarrow +\infty)| \approx 0.5$ (Fig. 11). This is the signature of relativistic bi-stability of the system [13, 14].

-
- [1] S. C. Wilks, J. M. Dawson, W. B. Mori, T. Katsouleas, and M. E. Jones, Phys. Rev. Lett. **62**, 2600 (1989); E. Esarey, A. Ting, and P. Sprangle, Phys. Rev. A **42**, 3526 (1990).
- [2] P. Gibbon and A. Bell, Phys. Rev. Lett. **61**, 1599 (1988); *ibid.* **61**, 2509 (1988); *ibid.* **65**, 1962 (1990); E. Esarey and A. Ting, *ibid.* **61**, 1961 (1990).
- [3] P. Gibbon, Phys. Fluids B **2**, 2196 (1990).
- [4] G. Shvets and A. Pukhov, Phys. Rev. E **59**, 001033 (1999).
- [5] N. E. Andreev, L. M. Gorbunov, V. I. Kirsanov, A. A. Pogosova, and A. S. Sakharov, Plasma Phys. Rep. **22**, 739 (1996).
- [6] G. Shvets, N. J. Fisch, A. Pukhov, and J. Meyer-ter-Vehn, Phys. Rev. Lett. **81**, 4879 (1998); V. M. Malkin, G. Shvets, and N. J. Fisch, Phys. Rev. Lett. **82**, 4448 (1999).
- [7] J. Faure, Y. Glinec, J. J. Santos, Phys. Rev. Lett. **95**, 205003 (2005).
- [8] M. N. Rosenbluth and C. S. Liu, Phys. Rev. Lett. **29**, 701 (1972).
- [9] T. Tajima and J. M. Dawson, Phys. Rev. Lett. **43**, 267 (1979).
- [10] C. M. Tang, P. Sprangle, and R. N. Sudan, Phys. Fluids **28**, 1974 (1985).
- [11] S. Ya. Tochitski, R. Narang, C. V. Filip *et al.*, Phys. Plasmas **11**, 2875 (2004); C. V. Filip, R. Narang, S. Ya. Tochitski *et al.*, Phys. Rev. E **69** 026404 (2004).
- [12] R. R. Lindberg, A. E. Charman, J. S. Wurtele, and L. Friedland, Phys. Rev. Lett. **93**, 055001 (2004).
- [13] G. Shvets, Phys. Rev. Lett. **93**, 195004 (2004).
- [14] S. Kalmykov, O. Polomarov, D. Korobkin, J. Otwinowski, J. Power, and G. Shvets, to appear in Philos. Trans. R. Soc. London, Ser. A (2005).

- [15] S. Kalmykov and G. Shvets, Phys. Rev. Lett., **94** 235001 (2005); S. Kalmykov, Bull. Am. Phys. Soc. **48**, 106 (2005).
- [16] W. B. Mori, IEEE J. Quantum Electron. **QE-33**, 1879 (1997).
- [17] C. Max, J. Arons, and B. Langdon, Phys. Rev. Lett. **33**, 209 (1974); I. Watts, M. Zepf, E. L. Clark *et al.*, Phys. Rev. E **66**, 036409 (2002).
- [18] W. B. Mori, C. D. Decker, D. E. Hinkel, and T. Katsouleas, Phys. Rev. Lett. **72**, 1482 (1994).
- [19] A. S. Sakharov and V. I. Kirsanov, Phys. Rev. E **49**, 3274 (1994).
- [20] B. I. Cohen, A. N. Kaufman, and K. M. Watson, Phys. Rev. Lett. **29**, 581 (1972).
- [21] S. J. Karttunen and R. R. E. Salomaa, Phys. Rev. Lett. **56**, 604 (1986); Physica Scr. **33**, 370 (1986).
- [22] S. E. Harris and A. V. Sokolov, *ibid.* **81**, 2894 (1998); Fam Le Kien, K. Hakuta, and A. V. Sokolov, Phys. Rev. A **66**, 023813 (2002).
- [23] D. Umstadter, E. Esarey, and J. Kim, Phys. Rev. Lett. **72**, 1224 (1994).
- [24] S. Dalla and M. Lontano, Phys. Rev. E **49**, R1819 (1994).
- [25] G. Bonnaud, D. Teychenné and J.-L. Bobin, Phys. Rev. E **50**, R36 (1994).
- [26] P. Mora, D. Pesme, A. Héron, G. Laval, and N. Silvestre, Phys. Rev. Lett. **61**, 1611 (1988).
- [27] L. M. Gorbunov, P. Mora, and T. M. Antonsen, Jr., Phys. Plasmas **4**, 4358 (1997).
- [28] Baiweh Li, S. Ishiguro, M. M. Škorić, Min Song, and T. Sato, Phys. Plasmas **12**, 103103 (2005).
- [29] E. Esarey, P. Sprangle, J. Krall, and A. Ting, IEEE Trans. Plasma Sci. **PS-24**, 252 (1996).
- [30] A. Yu. Goltsov, D. V. Korobkin, Y. Ping, and S. Suckewer, J. Opt. Soc. Am. B **17**, 868 (2000).
- [31] F. Grigsby, D. Peng, and M. Downer (private communication).